arXiv:1411.2016v2 [cond-mat.mes-hall] 12 Nov 2014

Quantum Anomalous Hall Effect in Magnetic Insulator Heterostructure

Gang Xu[1,2], Jing Wang[1], Claudia Felser[3], Xiao-Liang Qi[1], and Shou-Cheng Zhang[1]
[1] *Department of Physics, McCullough Building, Stanford University, Stanford, CA 94305-4045, USA*
[2] *Beijing National Laboratory for Condensed Matter Physics, and Institute of Physics, Chinese Academy of Sciences, Beijing 100190, China*
[3] *Max Planck Institute for Chemical Physics of Solids, Dresden, Germany*

(Dated: November 17, 2014)

Based on *ab initio* calculations, we predict that a monolayer of Cr-doped $(Bi,Sb)_2Te_3$ and GdI_2 heterostructure is a quantum anomalous Hall insulator with a non-trivial band gap up to 38 meV. The principle behind our prediction is that the band inversion between two topologically trivial ferromagnetic insulators can result in a non-zero Chern number, which offers a better way to realize the quantum anomalous Hall state without random magnetic doping. In addition, a simple effective model is presented to describe the basic mechanism of spin polarized band inversion in this system. Moreover, we predict that 3D quantum anomalous Hall insulator could be realized in $(Bi_{2/3}Cr_{1/3})_2Te_3$ /GdI_2 superlattice.

PACS numbers: 73.20.-r, 73.21.-b, 73.63.Hs, 72.25.Dc

The recent discovery of quantum anomalous Hall (QAH) effect has attracted tremendous interest in condensed matter physics [1–16]. In a QAH insulator, theoretically predicted in magnetic topological insulators (TIs) [1–5], the strong spin-orbit coupling and ferromagnetic (FM) ordering combine to give rise to an insulating state with a topologically nontrivial band structure characterized by a finite Chern number [17, 18]. Recently, the QAH effect has been experimentally observed in Cr-doped $(Bi,Sb)_2Te_3$ around 30 mK [9]. The robust dissipationless chiral edge states in the QAH state could be used for interconnects of semiconductor devices. Unfortunately, the topologically nontrivial band gap of this system is extremely small and the quantization of Hall conductance can only be observed below about 100 mK [15, 16]. For potential device applications, it is important to find materials for the QAH effect, and to increase the band gap as well as the Curie temperature (T_c) of magnetic moments.

The basic mechanism for the QAH effect is the band inversion between spin polarized bands in magnetic TIs. In this Letter, we propose a new class of materials to realize the QAH effect. Since the highest T_c in semiconductors is still far below room temperature, artificial materials are the only way. Layered crystals structures allow the production of monolayers and the synthesis of new compounds via combination of mono- and multilayers have been already demonstrated [19]. By combining two topologically trivial FM materials together, the topological insulator property arises from the relative spin polarized band inversion [20] between the two different FM materials of the thin films. In particular, based on first-principles calculations, for the interface between monolayer $(Bi,Sb)_2Te_3$ and GdI_2, we find that the spin polarized p_z-characterized conduction band from Cr-doped $(Bi,Sb)_2Te_3$ will invert with the spin polarized d_{z^2}-characterized valence band from Gd, resulting in a new QAH insulator with the non-trivial band gap up to 38 meV. As we know, GdI_2 is a halfmetallic ferromagnet, where the ferromagnetism is contributed by the transition metal element Gd and its Curie temperature T_c is around 300 K. A high T_c is thus expected for monolayer GdI_2 and $Cr_x(Bi,Sb)_{2-x}Te_3$ interface. All these proper-

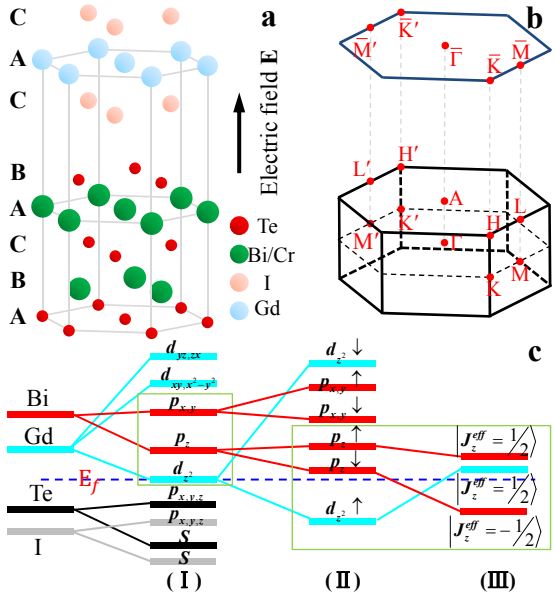

FIG. 1. (Color online) a, The crystal structure of monolayer Cr-doped Bi_2Te_3 and GdI_2 film. The black arrow indicate the electric field. b, The Brillouin zones (BZ) for the film (2D) and superlattice (3D) of triangle lattice, where high symmetry points Γ (0, 0, 0), $M(0, \pi, 0)$ and K $(2\pi/3, 2\pi/3, 0)$ are marked. c, The schematic picture of the origin of band structure in monolayer $(Bi_{1-x}Cr_x)_2Te_3/GdI_2$, starting from the atomic orbitals of Bi and Gd, the following three steps are required to understand the band structure: (I) the chemical bonding and crystal field effect, (II) the FM exchange coupling, and (III) SOC effect. E_f is the Fermi level (dashed line).

ties in this system are distinct from the previous proposals in magnetically doped TIs, such as Cr-doped Bi_2Se_3-family [5], where a high T_c and a large band gap are hard to achieve simultaneously.

Both $Cr_x(Bi,Sb)_{2-x}Te_3$ and GdI_2 are layered triangle lattice compounds interconnected along c-axis by van der Waals interactions, which makes their thin films chemically stable. $Cr_x(Bi,Sb)_{2-x}Te_3$ is a FM insulator with the in-plane lattice constant decreases from 4.35 Å to 4.15 Å as the content of Cr increases [21]. Experimentally, GdI_2 crystallizes in the well-known 2H-MoS_2 structure (194 space group), in which each Gd layer are sandwiched by two layers of I atoms with the trigonal prismatic geometry [22]. The in-plane lattice constant of GdI_2 is about 4.075 Å, resulting in a lattice mismatch 2% $\sim$ 6% (depending on the content of Cr) with $Cr_x(Bi,Sb)_{2-x}Te_3$. At room temperature, GdI_2 show a metallic behavior and FM transition with saturation magnetic moment about 7.33 μ_B/Gd, but becomes insulating at low temperature (below 150 K) [23]. Our calculations do find that the bulk of GdI_2 is a bad semimetal. However, for monolayer, it becomes insulating with a band gap about 0.2 eV, where the dispersions originated from the interlayer interaction are eliminated due to quantum confinement.

There are lots of stacking configurations to combine $Cr_x(Bi,Sb)_{2-x}Te_3$ and GdI_2 together. Comparing to other configurations, such as A(Te)-B(Bi/Cr)-C(Te)-A(Bi/Cr)-B(Te)-A(I)-C(Gd)-A(I), A(Te)-B(Bi/Cr)-C(Te)-A(Bi/Cr)-B(Te)-B(I)-A(Gd)-B(I) and A(Te)-B(Bi/Cr)-C(Te)-A(Bi/Cr)-B(Te)-C(I)-B(Gd)-C(I), we predict that the film shown in Fig. 1a, *i.e.* A(Te)-B(Bi/Cr)-C(Te)-A(Bi/Cr)-B(Te)-C(I)-A(Gd)-C(I) is the most stable one. Although there are some energy difference between different configurations, the electronic band structures of them look very similar. In addition, the site of Cr in $(Bi,Sb)_2Te_3$ also have very weak influence on the band structures. Therefore, we will focus on the configuration shown in Fig. 1a as representative in this paper.

We perform the first-principles density functional theory (DFT) [24, 25] calculations and PAW potentials [26, 27] by the Vienna Ab-initio Simulation Package (VASP) [28, 29]. Perdew-Burke-Ernzerhof-type [30] generalized gradient approximation + Hubbard U correction (DFT+U) [31, 32] with U = 6 eV (J = 0) on Gd's $4f$ orbitals and U = 3 eV (J = 1.5 eV) on Cr's $3d$ orbitals are used. The results are also double checked by HSE functional [33], which is known as more accurate description for the band structures of semiconductors. SOC effect is considered self-consistently in the calculations. The kinetic energy cut-off is fixed to 400 eV. 10×10×2/6×6×2 k-mesh are used for half doping and other Cr contents films respectively. For all the films, the vacuum region are thicker than 12 Å, and the lattice constants, as well as the atomic positions are fully optimized with the accuracy smaller than 0.01 eV/Å.

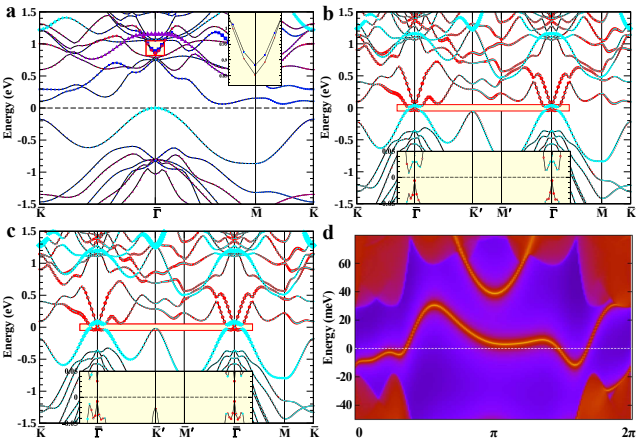

FIG. 2. (Color online) a, Spin-polarized band structures of $BiCrTe_3/GdI_2$ film without SOC, in which red circles and blue squares denote the projections to the down and up spin p_z orbital of Bi, while the cyan diamonds and purple triangles mean the projections to the up and down spin . The inset is the zoom-in of the red square region to show the magnetic splitting of p_z orbital. b and c, The band structures with SOC for $E = 0$ (no gating electric field) and $E = -0.1$ V/Åcase, where the projections to Bi p orbitals and Gd d_{z^2} orbital are indicated by red circles and cyan diamonds, respectively. The insets in b and c are the zoom-in around the Fermi level to show the insulating gap clearly. d, Calculated edge state of $BiCrTe_3/GdI_2$ based on the band structures shown in Fig. 2c. All Fermi levels are defined at 0 eV.

In Fig. 1c, we show a schematic picture of the origin of band inversion in monolayer $Cr_x(Bi,Sb)_{2-x}Te_3$ and GdI_2. Take the atomic energy levels of Bi ($6s^26p^3$), Gd ($4f^75d^16s^2$), Te($5s^25p^4$) and I($5s^25p^5$) as the starting point. At stage I, the chemical bonding and crystal field in Cr-doped $(Bi,Sb)_2Te_3$ and GdI_2 are considered separately: 1) In Cr-doped $(Bi,Sb)_2Te_3$, chemical bonding between Bi and Te push down all of the Te states, giving rise to the p-characterized valence bands of Te . On the other hand, the lifted up Bi p orbitals are split into two degenerate manifolds p_x, p_y and single p_z state by crystal field. After this splitting, the conduction band closest to the Fermi level (E_f) is the p_z state of Bi. 2) In GdI_2, chemical bonding push down all of the states of I far away from the Fermi level. Strong correlation effect split f orbitals of Gd into up and down Hubbard bands, which are far away from Fermi level too. So we neglect f states in this analysis. The trigonal prismatic coordination of the Gd atoms splits their d orbitals into three groups, d_{z^2}, $d_{xy}, d_{x^2-y^2}$ and d_{xz}, d_{yz}. With this splitting, the remaining one $5d$ electron of Gd half occupies on d_{z^2} state. At stage II, the d_{z^2} band of Gd split into two branches due to the magnetic polarization, making the up spin branch fully occupied and GdI_2 insulating. Because of the magnetic ordering of Cr, the p_z conduction band of Bi is split in a way that down spin branch moves

toward the Fermi level. Therefore, after the magnetic exchange interactions taking into account, the two bands closest to the Fermi level turn out to be $|d_{z^2},\uparrow\rangle$ (valence band) and $|p_z,\downarrow\rangle$ (conduction band) respectively. At the last stage III, after SOC effect are considered in, orbital and spin angular momenta mix together, while the total angular momentum is preserved. Therefore, $|p_z,\downarrow\rangle$ states becomes $\left|J_z^{\text{eff}}=-1/2\right\rangle$, which is very similar to the 'split off band' in the Kane model [34]. Due to the huge SOC effect of Bi, the energy of $\left|J_z^{\text{eff}}=-1/2\right\rangle$ will be dramatically dropped down and get inverted with $\left|J_z^{\text{eff}}=1/2\right\rangle$ state, which originated from $|d_{z^2},\uparrow\rangle$ of Gd. Because d orbital and p orbital have different parity, this kind of $d-p$ inversion at Γ point usually leads to non-trivial Berry's phase for the occupied bands. Therefore, the system becomes topologically non-trivial Chern insulator if a full band gap exists, and its Chern number is determined by ΔJ_z^{eff}, *i.e.* $C=1$.

Based on the analysis of the band sequence discussed above, a simple 2×2 model, with $|d_{z^2},\uparrow\rangle$ and $|p_z,\downarrow\rangle$ as the basis, can be introduced to describe the spin polarized band inversion,

$$H_{\text{eff}}=\begin{pmatrix} M & Dk_- \\ Dk_+ & -M \end{pmatrix} \tag{1}$$

where $k_\pm=k_x\pm ik_y$, and $M=M_0-B(k_x^2+k_y^2)$ is the mass term expanded to the second order, with parameters $M_0>0$ and $B>0$ to ensure the band inversion. Since the two bases have opposite parity, the off-diagonal element has to be odd in k. In addition, it has to have the form of $k_\pm$ to conserve the angular momentum along the z direction.

In order to justify this effective model, we have performed the first principles calculations on the $(Bi_{1-x}Cr_x)_2Te_3/GdI_2$ films. First, we focus on the half doping case, and show its spin-polarized band structures (without SOC) in Fig. 2a. Our calculations confirm that the magnetic moments on Cr and Gd prefer ferromagnetic arrangement with 0.33 meV lower than antiferromagnetic configuration. The calculated moments are 3.20 μ_B/Cr and 7.48 μ_B/Gd, similar to previous calculations [5, 35] and measurements [23]. As shown in Fig. 2a, one single-layer $BiCrTe_3$ is a normal insulator due to the confinement effect, in which the conduction bands from Bi and Cr are well separated with the valance band from Te by a gap about 0.6 eV. Within this gap lies an occupied spin-up band of Gd, making $BiCrTe_3/GdI_2$ film as a narrow gap insulator if SOC is not considered.

Next, we carry fully relativistic calculations, to study the influence of SOC on the electronic structures by aligning the magnetic moments perpendicular to the film, since the direction of magnetic moment in Cr-doped $(Bi,Sb)_2Te_3$ is confirmed to be along c-axis [9, 21]. In the presence of SOC, $|d_{z^2},\uparrow\rangle$ of Gd becomes $\left|J_z^{\text{eff}}=1/2\right\rangle$. Meanwhile, p_z orbitals evolve into two 'spin hole' like

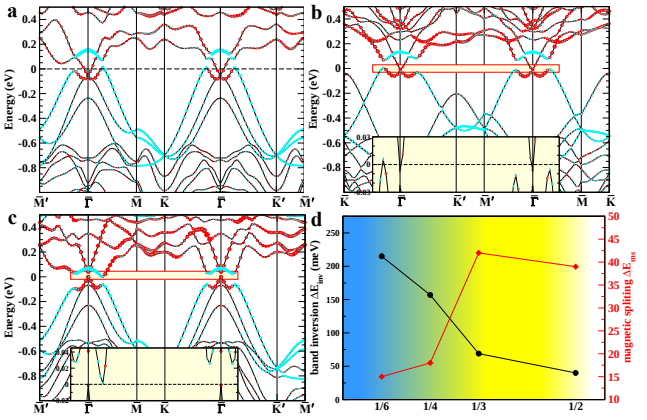

FIG. 3. (Color online) a, b and c show the band structures with SOC for 1/6, 1/4 and 1/3 Cr-doped Bi_2Te_3 and GdI_2 films. The size of red circles and cyan diamonds mean the projections to Bi p orbitals and Gd d_{z^2} orbital respectively. The insets in b and c are the zoom-in of the red square region around the Fermi level. All Fermi levels are defined at 0 eV. d, The schematic phase diagram of Cr-doped Bi_2Te_3 and GdI_2 films, in which the yellow region on right side means the Chern insulator, the blue region on left side indicates the topological metal. Among of them, the transition region means the tunable topological semi-metal.

bands by reconstruction with p_x and p_y orbitals. Because inversion symmetry is broken in this system, these two 'spin hole' like bands show large Rashba splitting, resulting in one inner band and one outer band with W-shape around $\bar{\Gamma}$ point. The outer and inner bands are further split at $\bar{\Gamma}$ point due to magnetic exchange interactions. Approximately, the inner band is called $\left|J_z^{\text{eff}}=1/2\right\rangle$, since it contains $|p_z,\uparrow\rangle$ component at $\bar{\Gamma}$ point; the outer band, which originated from $|p_z,\downarrow\rangle$, is defined as $\left|J_z^{\text{eff}}=-1/2\right\rangle$; the energy difference between the inner band ($\left|J_z^{\text{eff}}=1/2\right\rangle$) and outer band ($\left|J_z^{\text{eff}}=-1/2\right\rangle$) at $\bar{\Gamma}$ point is defined as ΔE_{ms}. Our calculations suggest $\Delta E_{\text{ms}}=39$ meV at Cr half doping case. Comparing with Fig. 2a, huge SOC effect of Bi drops down the 'spin hole' like bands dramatically. As shown in Fig. 2b, even though there is still a normal gap bigger than 0.5 eV between Bi's p orbitals and Te's p orbitals, the $\left|J_z^{\text{eff}}=-1/2\right\rangle$ band from Bi is inverted with $\left|J_z^{\text{eff}}=1/2\right\rangle$ band from Gd at $\bar{\Gamma}$ point, and re-open an insulating gap about 15 meV. According to our previous analysis, this kind of $d-p$ band inversion can give rise to a topological non-trivial Chern insulator. We note that, due to both time reversal symmetry and inversion symmetry are broken in ferromagnetic $BiCrTe_3/GdI_2$ film, the band structures along $\bar{\Gamma}$-$\bar{K}$ and $\bar{\Gamma}$-$\bar{K}'$ directions show different behavior in Fig. 2b and Fig. 2c.

Another advantage of the freestanding films is that one can modulate the band inversion continuously by an external gating electric field E [36]. In Fig. 2c, we show the well-modulated band structures of $BiCrTe_3/GdI_2$ film by $E=-0.1$ V/Å, in which the optimal topological insu-

lating gap 38 meV is achieved. In order to confirm the system's topological properties, we carry out the calculations of edge states by constructing the Green functions [37] for the semi-infinite edge based on Maximally Localized Wannier functions method [38, 39]. The results based on the band structures with optimal gap (Fig. 2c) are shown in Fig. 2d, in which one topologically protected chiral edge state connecting $\left|J_z^{\text{eff}}=1/2\right\rangle$ and $\left|J_z^{\text{eff}}=-1/2\right\rangle$ presents clearly, consistent with our previous analysis that $C=1$.

We also perform calculations on systems with other Cr contents, such as 1/6, 1/4, 1/3 doping, trying to study the topological properties as a function of Cr doping. The results are shown in Fig. 3. Our calculations suggest that, at 1/3 doping case, the system is also Chern insulator with a small gap about 3.6 meV (see Fig. 3c), in which the magnetic splitting at $\bar{\Gamma}$ point ΔE_{ms} is about 44 meV, a little enhanced than half doping case. However, when Cr content keeps decreasing, the magnetic splitting ΔE_{ms} becomes smaller and smaller (see Fig. 3d), while the band inversion between $\left|J_z^{\text{eff}}=1/2\right\rangle$ from Gd and $\left|J_z^{\text{eff}}=-1/2\right\rangle$ from Bi becomes deeper and deeper. Therefore both the cases of 1/4 and 1/6 doping are topologically non-trivial semimetal, in which both valence band and conduction band are partially occupied at different momentum k (see Fig. 3a and Fig. 3b). We summarize the topological properties evolution with Cr content in Fig. 3d, in which ΔE_{inv} is defined by the energy level of $\left|J_z^{\text{eff}}=1/2\right\rangle$ from Gd minus the energy level of $\left|J_z^{\text{eff}}=-1/2\right\rangle$ from Bi. As shown in Fig. 3d, one can find that: 1) Band inversion ΔE_{inv} increases monotonically with the decrease of Cr concentration, which is because of the 'split off' bands dropping deeper and deeper due to the increased SOC effect [40]. 2) Magnetic splitting ΔE_{ms} is mainly decreasing when the Cr concentration becomes smaller. This is consistent with the fact that Curie temperature T_c decreases with Cr concentration reduction in experiment [21]. As a result, when $x>1/3$, *i.e.* the yellow region on right side in Fig. 3d, $(Bi_{1-x}Cr_x)_2Te_3/GdI_2$ films are the Chern insulator, in which QAH effect can be realized. In contrast, with the weekly doping $x<1/6$, *i.e.* the blue region on left side in Fig. 3d, the system is topological metal with $d-p$ band inversion. Between them, the transition region indicates the tunable topological semi-metal, which means one can modulate this semi-metal to a Chern insulator by applying experimentally reasonable gate voltage or by Sb doping. Take 1/4 doping as an example, by applying electric gating field $E=0.2$ V/Å, a Chern insulator with a gap about 18 meV can be achieved.

Finally we would like to address the topological properties of the superlattice. Because Cr-doped $(Bi,Sb)_2Te_3$ and GdI_2 are coupled by the van der Waals interactions along z-direction, the dispersion of the supperlattice along k_z is very weak. If the $d-p$ band inversion is big enough, making all k_z-plane's Chern number equaling 1, such system can be called 3D Chern insulator [6]. Here we show the calculated band structures on $(Bi_{2/3}Cr_{1/3})_2Te_3$ /GdI_2 supperlattice in Fig. 4a, where the $\left|J_z^{\text{eff}}=-1/2\right\rangle$ state from Bi is always lower than the $\left|J_z^{\text{eff}}=1/2\right\rangle$ state from Gd at all k_z and a full insulating gap about 8 meV present. This indicates that 3D Chern insulator is realized in $(Bi_{2/3}Cr_{1/3})_2Te_3$ /GdI_2 supperlattic, which can be confirmed by the edge state calculations for $k_z=0$ and $k_z=\pi$ plane (shown in Fig. 4c and 4d). On the other hand, if we tune ΔE_{inv} to a suitable size, making that the $d-p$ band inversion only happens at Γ point while A point ($k_z=\pi$) remains a normal insulating gap, the system will be a nontrivial semimetal with topologically unavoidable Weyl nodes [6] located at the phase boundary separating $C=1$ and $C=0$ planes. In Fig. 4b, we show the numerical results on $(Sb_{2/3}Cr_{1/3})_2Te_3$ /GdI_2 supperlattice, confirming that such topologically unavoidable Weyl node form in it, even though the Weyl nodes do not cross the Fermi level due to some d bands from Cr are dropping below E_f in $(Sb_{2/3}Cr_{1/3})_2Te_3$.

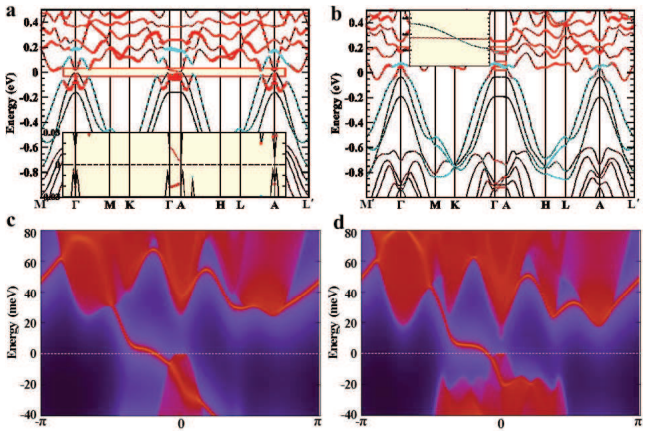

FIG. 4. (Color online) a and b show the band structures with SOC for $(Bi_{2/3}Cr_{1/3})_2Te_3$ and $(Sb_{2/3}Cr_{1/3})_2Te_3$ superlattice respectively. The size of red circles and cyan diamonds mean the projections to Bi p orbitals and Gd d_{z^2} orbital respectively. The insets in a is the zoom-in of the red square region around the Fermi level. The insets in b is the zoom-in of the red square region to show Weyl node. c and d is the d calculated edge state of $(Bi_{2/3}Cr_{1/3})_2Te_3$ superlattice for $k_z=0$ and $k_z=\pi$ plane respectively. The Fermi levels are defined at 0 eV.

This work is supported by the US Department of Energy, Office of Basic Energy Sciences, Division of Materials Sciences and Engineering under Contract No. DE-AC02-76SF00515, and by the Defense Advanced Research Projects Agency Microsystems Technology Office, MesoDynamic Architecture Program (MESO) through contract numbers N66001-11-1-4105, and partly by FAME, one of six centers of STARnet, a Semiconductor Research Corporation program sponsored by MARCO and DARPA. G.X. would like to thank for the support

from 973 program of China (No.2013CB921704) and NSF of China.

[1] X. L. Qi, Y. S. Wu, and S. C. Zhang, Phys. Rev. B **74**, 045125 (2006).
[2] X.-L. Qi, T. Hughes, and S.-C. Zhang, Phys. Rev. B **78**, 195424 (2008).
[3] C.-X. Liu, X.-L. Qi, X. Dai, Z. Fang, and S.-C. Zhang, Phys. Rev. Lett. **101**, 146802 (2008).
[4] R. Li, J. Wang, X. L. Qi, and S. C. Zhang, Nature Phys. **6**, 284 (2010).
[5] R. Yu, W. Zhang, H. J. Zhang, S. C. Zhang, X. Dai, and Z. Fang, Science **329**, 61 (2010).
[6] G. Xu, H. Weng, Z. Wang, X. Dai, and Z. Fang, Phys. Rev. Lett. **107**, 186806 (2011).
[7] D. Xiao, W. Zhu, Y. Ran, N. Nagaosa, and S. Okamoto, Nat. Commun. **2**, 596 (2011).
[8] A. Rüegg and G. A. Fiete, Phys. Rev. B **84**, 201103 (2011).
[9] C.-Z. Chang, J. Zhang, X. Feng, J. Shen, Z. Zhang, M. Guo, K. Li, Y. Ou, P. Wei, L.-L. Wang, Z.-Q. Ji, Y. Feng, S. Ji, X. Chen, J. Jia, X. Dai, Z. Fang, S.-C. Zhang, K. He, Y. Wang, L. Lu, X.-C. Ma, and Q.-K. Xue, Science **340**, 167 (2013).
[10] J. Wang, B. Lian, H. Zhang, Y. Xu, and S.-C. Zhang, Phys. Rev. Lett. **111**, 136801 (2013).
[11] J. Wang, B. Lian, H. Zhang, and S.-C. Zhang, Phys. Rev. Lett. **111**, 086803 (2013).
[12] H. Zhang, J. Wang, G. Xu, Y. Xu, and S.-C. Zhang, Phys. Rev. Lett. **112**, 096804 (2014).
[13] K. F. Garrity and D. Vanderbilt, Phys. Rev. B **90**, 121103 (2014).
[14] J. Wang, B. Lian, and S.-C. Zhang, Phys. Rev. B **89**, 085106 (2014).
[15] X. Kou, S.-T. Guo, Y. Fan, L. Pan, M. Lang, Y. Jiang, Q. Shao, T. Nie, K. Murata, J. Tang, Y. Wang, L. He, T.-K. Lee, W.-L. Lee, and K. L. Wang, Phys. Rev. Lett. **113**, 137201 (2014).
[16] J. G. Checkelsky, R. Yoshimi, A. Tsukazaki, K. S. Takahashi, Y. Kozuka, J. Falson, M. Kawasaki, and Y. Tokura, Nat. Phys. **10**, 731 (2014).
[17] D. J. Thouless, M. Kohmoto, M. P. Nightingale, and M. den Nijs, Phys. Rev. Lett. **49**, 405 (1982).
[18] F. D. M. Haldane, Phys. Rev. Lett. **61**, 2015 (1988).
[19] A. K. Geim and I. V. Grigorieva, Nature **499**, 419 (2013).
[20] C.-X. Liu, T. L. Hughes, X.-L. Qi, K. Wang, and S.-C. Zhang, Phys. Rev. Lett. **100**, 236601 (2008).
[21] Z. Zhou, Y.-J. Chien, and C. Uher, Phys. Rev. B **74**, 224418 (2006).
[22] A. Kasten, P. Muller, and M. Schienle, Solid State Communications **51**, 919 (1984).
[23] K. Ahn, C. Felser, R. Seshadri, R. Kremer, and A. Simon, Journal of Alloys and Compounds **303-304**, 252 (2000).
[24] P. Hohenberg and W. Kohn, Phys. Rev. **136**, B864 (1964).
[25] W. Kohn and L. J. Sham, Phys. Rev. **140**, A1133 (1965).
[26] P. E. Blöchl, Phys. Rev. B **50**, 17953 (1994).
[27] G. Kresse and D. Joubert, Phys. Rev. B **59**, 1758 (1999).
[28] G. Kresse and J. Hafner, Phys. Rev. B **47**, 558 (1993).
[29] G. Kresse and J. Furthmüller, Phys. Rev. B **54**, 11169 (1996).
[30] J. P. Perdew, K. Burke, and M. Ernzerhof, Phys. Rev. Lett. **77**, 3865 (1996).
[31] V. I. Anisimov, J. Zaanen, and O. K. Andersen, Phys. Rev. B **44**, 943 (1991).
[32] S. L. Dudarev, G. A. Botton, S. Y. Savrasov, C. J. Humphreys, and A. P. Sutton, Phys. Rev. B **57**, 1505 (1998).
[33] J. Heyd, G. E. Scuseria, and M. Ernzerhof, The Journal of Chemical Physics **118**, 8207 (2003).
[34] L. C. L. Y. Voon and M. Willatzen, *The kp method: Electronic Properties of Semiconductors* (Springer, Berlin, 2009).
[35] J.-M. Zhang, W. Ming, Z. Huang, G.-B. Liu, X. Kou, Y. Fan, K. L. Wang, and Y. Yao, Phys. Rev. B **88**, 235131 (2013).
[36] X. Kou, M. Lang, Y. Fan, Y. Jiang, T. Nie, J. Zhang, W. Jiang, Y. Wang, Y. Yao, L. He, *et al.*, ACS nano **7**, 9205 (2013).
[37] M. L. Sancho, J. L. Sancho, J. L. Sancho, and J. Rubio, Journal of Physics F: Metal Physics **15**, 851 (1985).
[38] N. Marzari and D. Vanderbilt, Phys. Rev. B **56**, 12847 (1997).
[39] I. Souza, N. Marzari, and D. Vanderbilt, Phys. Rev. B **65**, 035109 (2001).
[40] J. Zhang, C.-Z. Chang, P. Tang, Z. Zhang, X. Feng, K. Li, L.-l. Wang, X. Chen, C. Liu, W. Duan, K. He, Q.-K. Xue, X. Ma, and Y. Wang, Science **339**, 1582 (2013).